4418 *Macromolecules* **2010**, *43*, 4418–4427
DOI: 10.1021/ma1003997

Macromolecules
ARTICLE

Simulations of Terminally Charged Dendrimers with Flexible Spacer Chains and Explicit Counterions

J. S. Kłos*,†,§ and J.-U. Sommer†,‡

†*Leibniz Institute of Polymer Research Dresden e. V., 01069 Dresden, Germany,*
‡*Institute for Theoretical Physics, Technische Universität Dresden, 01069 Dresden, Germany, and*
§*Faculty of Physics, A. Mickiewicz University, Umultowska 85, 61-614 Poznań, Poland*

Received March 1, 2010; Revised Manuscript Received March 28, 2010

ABSTRACT: We study the properties of terminally charged dendrimers under systematic variation of the length of flexible spacers, accompanied by explicit counterions in an athermal solvent using Monte Carlo simulations based on the bond fluctuation model. In our study, both the full Coulomb potential and the excluded volume interactions are taken into account explicitly with the reduced temperature, τ, as the main control parameter. Our calculations confirm that counterions get localized in the molecules' interior and, in particular, condense on the terminal groups as τ is lowered. This, in turn, affects the conformational properties of the molecules that swell at intermediate τ due to dominating repulsion between the terminal groups and shrink in the limit of high and low τ, respectively. Like for neutral dendrimers, we find a substantial decrease in monomer densities with the radial distance from the dendrimers' center of mass and backfolding of the terminal groups toward the molecules' interior. By means of the radius of gyration tensor, we conclude that the mean instantaneous shape of dendrimers is spherical for all τ inspected.

I. Introduction

Research on charged dendrimers is inspired by a fair range of promising applications of these highly branched molecules in technology, materials engineering, biomedicine and pharmacy. Dendrimers have already been used to deliver oligonucleotides to the cell,[1,2] they enhance cytosolic and nuclear availability as indicated by confocal microscopy as well as cell uptake and transfection efficiency of plasmid DNA.[3] Guest−host nanodevices such as gold/PAMAM (polyamidoamine-dendrimers) nanocomposites are potentially very useful agents for improving the imaging and radiation treatment of cancer. It has been shown that the modulation of the surface charge and composition changes the in vivo biodistribution characteristics and toxicology of the nanodevices.[4]

Physical properties of charged dendrimers, their molecular conformation and structure have been the subject of experimental studies as well.[5−8] For instance, small-angle X-ray scattering (SAXS) and conductivity measurements have been made for dilute solutions of PAMAM molecules with univalent and divalent counterions.[5] Among others the latter have shown that divalent counterions are more strongly condensed on the dendrimers and thus more effective in reducing their charge. As indicated by small-angle neutron scattering (SANS), SAXS, and transmission electron microscopy (TEM) PAMAM dendrimers are useful for forming gold nanoclusters within their interior.[9,10] A number of EPR and UV−vis spectroscopy measurements have demonstarated that at various temperatures and pH divalent metal ions can be distributed both inside and outside the molecule.[11,12] Furthermore, apart from dendrimers' ability to encapsulate smaller molecules, with the use of optical reflectometry, atomic force microscopy (AFM), light scattering, SANS, and electrophoretic mobility measurements a number of recent works have been devoted to their adsorption properties on silica surfaces and latex particles as well as to formations of defined supramolecular assemblies based on ionic interaction in aqueous solution.[13−16]

It is generally accepted that explicit treatment of counterions is necessary for the theoretical explanation of the structure and conformations of linear polyelectrolytes[17−31] as well as terminally charged dendrimers.[32−46] In particular computational studies indicate that condensation of ions on dendrimers occurs with increasing strength of the electrostatic interactions and is accompanied by subsequent swelling and shrinking of the molecules.[41,43−46] Counterions themselves penetrate not only the dendrimers' periphery but also the interior, and for very strong electrostatic couplings their density practically overlaps with that of terminal groups.[40,41] It has been shown that ions tremendously affect interactions between likely charged dendrimers that can even become attractive.[47,48] Furthermore, some of the latest studies with explicit counterions have concentrated on such crucial issues as structural properties of charged half-generation PAMAMs, complexes comprised of charged dendrimers and linear polyelectrolytes, self-organization in solutions of charged dendrimers, the effect of chargeable monomers and valency of salt on the molecules' conformation and dynamics of counterions in dendrimer polyelectrolyte solutions.[49−56]

Because of high computational costs of simulating charged dendrimers a number of important studies on dendrimers' properties in solvents of various ionic strengths have been carried out using the Debye−Hückel approximation.[57,58] The Brownian dynamics method applied within this kind of approach has led to interesting results concerning dynamic properties (self-diffusion, rotational mobility, dendrimer elastic motions, etc.) of dilute solutions of charged dendrimers and adsorption of the molecules onto oppositely charged flat surfaces.[59,60] The very first approach to examine charged dendrimer-linear polyelectrolyte complexes has been made as well.[61−64] Furthermore, the structure of flexible chain dendrimers with long spacers comprising some fraction of charged monomers has been studied by a combination of the Flory-type analysis and numerical self-consistent-field calculations.[65]

*Corresponding author.

 Published on Web 04/09/2010

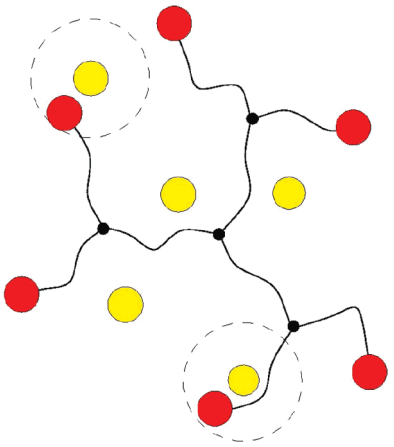

Figure 1. Schematic 2D picture of dendrimers. The terminal groups (counterions) are shown with the red (yellow) spheres. Condensed counterions are indicated by dashed circles.

In this work, we study the effect of spacer length variation on terminally charged dendrimers in good solvent with explicit counterions that model PAMAMs in aqueous environments at neutral pH values.[41,49,54] In particular, we investigate the interplay between charge effects and spacer-length scaling. The latter has been demonstrated for neutral dendrimers in our previous work.[66] To investigate spacer length variations large molecules up to 2146 flexible units are simulated using the bond fluctuation model (BFM). To the best of our knowledge this is the first application of the BFM to such highly branched polyelectrolytes, which proves efficient and enables a systematic inspection of large molecules on the coarse-grained level.

The remaining part of the article is organized as follows. In Section II we outline the model and the simulation method. The results of our simulations are presented and discussed in Section III. Finally, our conclusions and remarks are given in Section IV.

II. Model and Simulations

In the present work, we carry out Monte Carlo simulations using the bond fluctuation method on a cubic lattice.[67,68] We benefit from the advantages of this algorithm, which by definition secures the excluded volume condition and prevents the bonds from crossing. It is suited for simulations of linear chains as well as molecules with a highly branched architecture of their skeleton. In particular, for the latter molecules, the algorithm enables proper moves both for monomers constituting linear parts of the molecules and for the branches.

The systems of interest contain single dendrimers with movable centers and counterions. In the simulations, a cubic box of the size $L^3 = 500 \times 500 \times 500u^3$ (where u is the lattice unit) is used with periodic boundary conditions under all three dimensions. The molecules are modeled as treelike collections of beads connected by the BFM lattice bonds so as to form the macromolecular skeleton. (For a 2D schematic representation of dendrimers, see Figure 1.)

Before actual simulation runs, dendrimers of generation $G = 5, 6$, spacer length $S = 1, 2, 4, 8$, and branching functionality $f = 3$ are generated by a divergent growth process in the ascending order of the internal generation number $0 \le g \le G$ starting from the core of two bonded monomers. Thus, the molecules consist of

$$N = 2 + 4S(2^G - 1) \tag{1}$$

monomers,

$$N_t = 2^{G+1} \tag{2}$$

of which are the terminal groups that carry positive charges of valence $z = 1$. To guarantee charge neutrality of the systems, additional N_t free beads mimic counterions that bear negative charges $z = -1$. Thus, there are $N_m = N + N_t$ movable elements in the system, and the electrostatic interaction between the charges is the total Coulomb energy

$$E(r_{ij}) = \frac{E_c(r_{ij})}{\delta} = \frac{z_i z_j}{r_{ij}} \tag{3}$$

where r_{ij} is the distance between the ith and jth ions with valences z_i and z_j. The energy unit is defined as

$$\delta = \frac{e^2}{\varepsilon u} \tag{4}$$

where e stands for the electric charge and ε stands for the permittivity of the solvent. The long-range nature of the Coulomb interactions is treated by the Ewald summation method with the minimum image convention for the real-space term, $\kappa = 5/L, k_{max} = 6$ for the sum in the reciprocal space and for a conducting external medium. (See Appendix A.)[69,70] We calculate thermodynamic averages at the reduced temperature $\tau = k_B T/\delta$, where T is the absolute temperature and k_B is the Boltzmann constant. The model can be converted to real units by the inverse relation

$$\tau = \frac{u}{\lambda_B} \tag{5}$$

between τ and the Bjerrum length, $\lambda_B = e^2/\varepsilon k_B T$. For instance, the choice of $u \approx 2$ Å corresponds within the BFM with the bond length, $a \approx 5$ Å, which in turn corresponds reasonably to real dendrimers.[71] In water at room temperatures where $\lambda_B \approx 7$ Å, eq 5 yields then $\tau \approx 0.3$.

Configurations are sampled using the BFM model. (For details, see ref 66.) A new configuration is accepted or rejected according to a probability of the Metropolis type[72]

$$p = \min[1, \exp(-\Delta E/\tau)] \tag{6}$$

with $\Delta E = E_{new} - E_{old}$. ($E_{new}$ and E_{old} are energies after and before a random reconfiguration, $E = E_c/\delta$.) In our studies, the systems were equilibrated for a maximum of 10^7 MCS (Monte Carlo steps; one MCS consists of N_m random selections of monomers to be moved in a randomly chosen, one of the six directions by a single lattice unit), whereas averages were calculated for 10^3 to 10^4 equilibrium configurations stored every 10^3th MCS.

III. Results

A. Counterion Condensation. The phenomenon of counterion condensation has been introduced by Manning in his studies on an infinite cylindrical polyelectrolyte with linear charge density.[22−25] It refers to effective renormalizing the linear charge density by a fraction of counterions that get localized very near the molecule but do not recombinate. Obviously, this phenomenon is more difficult to be handled for the complex shapes of molecules, in particular, for the present case, where only the terminal groups are charged.

The tendency of counterions to concentrate around the terminal groups in our simulated systems can be demonstrated by the end-group−counterion pair correlation function, g_{ec}, as shown in Figure 2. Sharp peaks observed in g_{ec} correspond to pronounced condensation. Note that our simulations show that at given τ and G, condensation is more significant for shorter spacers. The disappearance of the peak for higher temperature signals delocalization of the counterions. Besides this "strong" condensation effect of

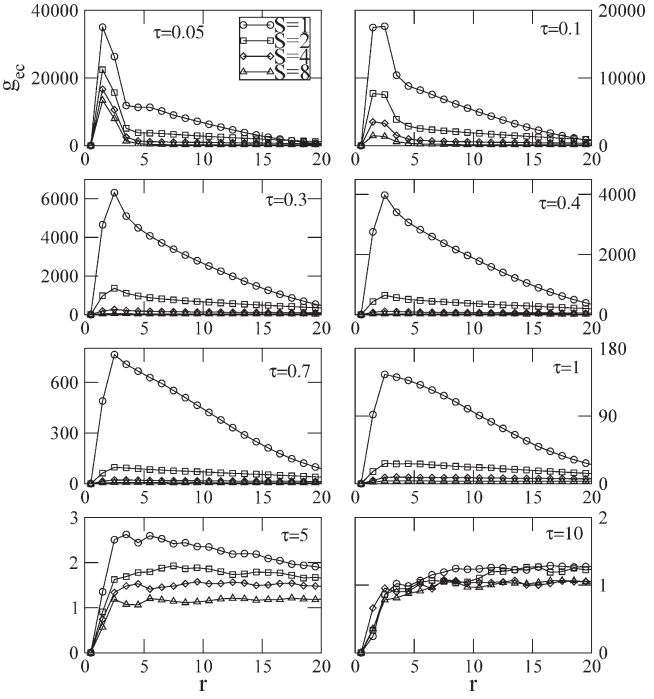

Figure 2. End-group−counterion pair correlation function for $G = 5$, fixed τ, and variable spacer length.

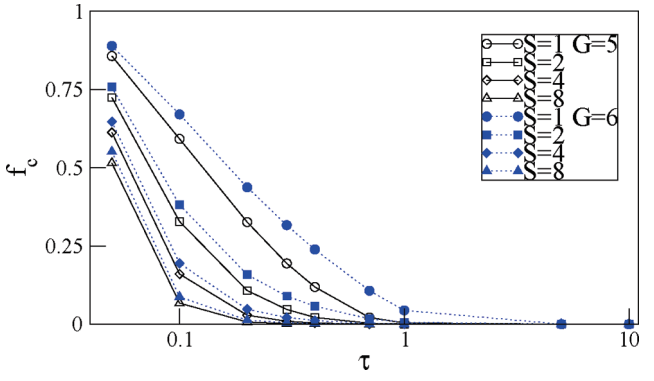

Figure 3. Fraction f_c of condensed counterions versus τ.

counterions at the charged groups, there is a "weak" localization of counterions due to the dendrimer as a whole (being essentially a spherical charge on larger distances). This effect will be discussed in Section IIID in more detail. Note that the peak in the pair correlation function for lower temperatures is not shifted, except at the lowest temperature where practically all counterions are localized.

To quantify the amount of condensed counterions, we adapt the simplest criterion for condensation based on the distance between ions and charged beads. More specifically, throughout the article, it is assumed that an ion is condensed when its distance from at least one end bead is less than $\sqrt{6}$, which is comparable to the average bond length of the BFM. Although this kind of approach is connected to some arbitrariness in choosing the actual radius of condensation, it is widely used in studies on polyelectrolyte systems and has proven to be reasonable for both lattice and off-lattice simulations.[41,44−46,73] For a general comparison of various methods, we refer to the work by K. Grass and C. Holm.[73] Note that our observation of the nearly constant peak position of the correlation functions in Figure 2 confirms this approach. In Figure 3, we plot the normalized fraction

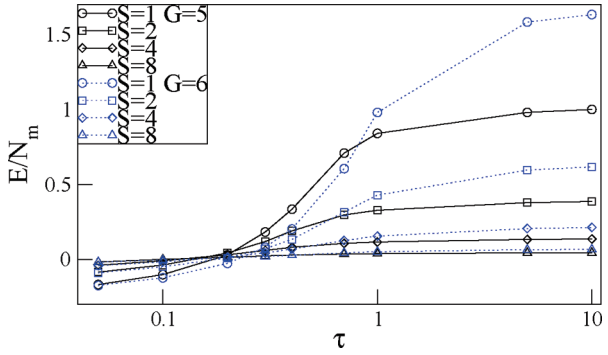

Figure 4. Mean total Coulomb energy per monomer E/N_m versus τ. The solid (dotted) lines correspond to $G = 5$ ($G = 6$).

$f_c = \langle N_c \rangle / N_t$ of condensed counterions on the terminal groups as a function of τ, where $\langle N_c \rangle$ denotes the mean absolute number of condensed counterions. It is seen that f_c increases monotonically with decreasing τ from nearly zero in the high-temperature limit to some finite values in the other extreme, which in turn proves that the phenomenon of condensation takes place. We note that using the Bjerrum length, $\lambda_B = u/\tau$, for the cutoff would sharpen the decay of $f_c(\tau)$ in Figure 3 (decreasing even the range for higher temperatures where less counterions are condensed).

At the lowest $\tau = 0.05$, nearly 90% of counterions are condensed for $S = 1$, whereas only ~50% are condensed for $S = 8$. Furthermore, as indicated by Figure 3, an increase in the generation number, G, leads to a small increase in f_c for fixed τ and S. Thus, we confirm that the phenomenon of ion condensation on the terminal groups is of generic nature and independent of the models used. Similar behavior of counterions with varying strength of electrostatic interactions has been found by both molecular dynamics and Monte Carlo simulations of terminally charged dendrimers with single spacers, $S = 1$.[41,44] Note that ion condensation is accompanied by a monotonic decrease in the mean total Coulomb energy, E, as displayed in Figure 4. It is worth noticing that the states with almost perfect condensation have negative energies.

B. Radius of Gyration. To analyze the size of charged dendrimers, we consider the mean square radius of gyration

$$\langle R_g^2 \rangle = \left\langle \frac{1}{N} \sum_{i=1}^{N} (r_i - r_{cm})^2 \right\rangle \tag{7}$$

where r_i and r_{cm} are the position vectors of the ith monomer and of the center of mass (c.m.) of the dendrimer, respectively. In the following, we use the shorthand notation, $R_g = (\langle R_g^2 \rangle)^{1/2}$. For neutral dendrimers, mean-field approximation of excluded volume effects leads to spacer length scaling, as we have shown in our previous work.[66] In particular, we can write

$$R_{g0}/S^{\nu} \approx (nG^2)^{1/5} \tag{8}$$

where $\nu = 3/5$ denotes the Flory exponent and $n = N/S$ is the number of spacer chains. The extension of spacers $R_S \approx S^{\nu}$ and self-density $S/R_s^3 \approx S^{1-3\nu}$ set the characteristic length scale and monomer density of dendrimers of given generation, G, respectively. In ref 66, we have found very good agreement of spacer length scaling with the results for R_{g0} as well as for the density profiles. Moreover, we have explicitly shown the independence of the average extension of spacers of the generation of the dendrimer.

For the charged dendrimer, we expect deviations from eq 8 due to electrostatic interactions, which tend to swell the

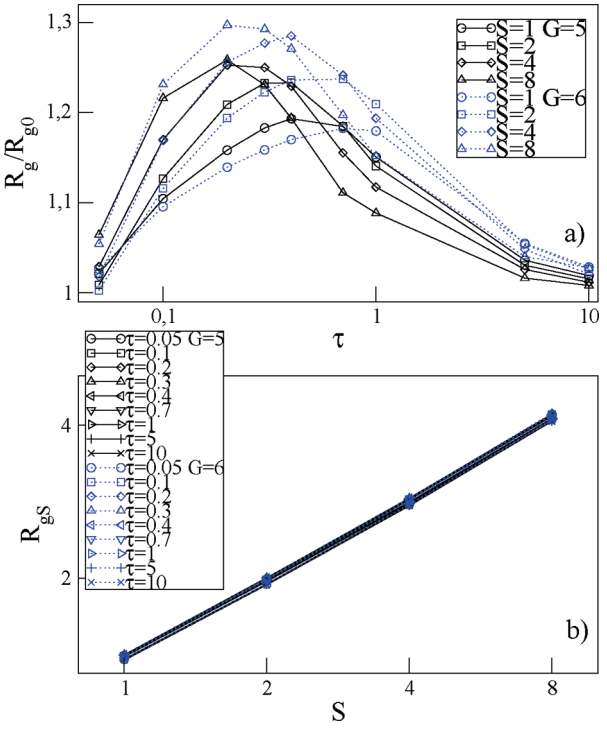

Figure 5. (a) Aspect ratio, R_g/R_{g0}, between the radius of gyration of charged and neutral dendrimers versus τ. (b) Mean radius of gyration of spacers, R_{gS}, versus spacer length, S, at the considered τ. The solid (dotted) lines correspond to $G = 5$ ($G = 6$).

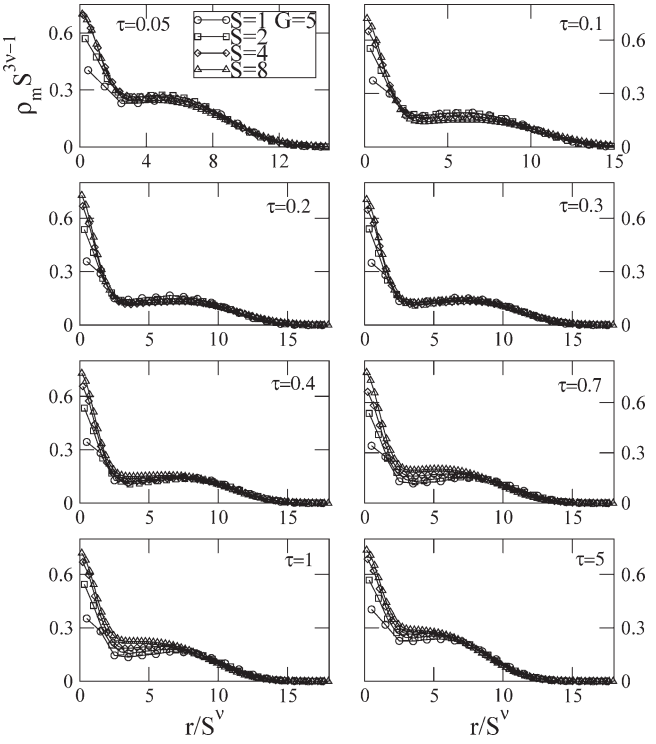

Figure 6. Rescaled radial monomer density ρ_m versus the rescaled distance from the dendrimers' c.m. at various τ for $G = 5$.

dendrimer. In Figure 5a, we show the rescaled radius of gyration, R_g/R_{g0}, as a function of τ. In accordance with previous studies on terminally charged dendrimers,[40,41,44] R_g displays a nonmonotonous behavior with respect to τ. In the limit of both high and low temperatures, R_g becomes comparable to the radius of gyration, R_{g0}, of the uncharged molecule. (See ref 66.) Actually, it is seen that the molecule shrinks to comparable sizes in the extremes of very high and very low τ, whereas at intermediate temperatures, it swells up. The maximal extension of the charged dendrimer as compared with the neutral dendrimer with the same G and S drops from around 1.3 for $S = 8$ to 1.2 for $S = 1$. Because deviations of the curves for various spacer lengths and generations in Figure 5a are in the range of 10%, we can only approximately assume the relation

$$R_g \approx A(\tau) R_{g0} \tag{9}$$

Combining eqs 8 and 9 yields

$$R_g/S^{\nu} \approx A(\tau)(nG^2)^{1/5} \tag{10}$$

The right-hand side of the above equation is independent of S because the number of spacer chains is defined only by the functionality and the number of generations, G. Therefore, roughly speaking, like neutral dendrimers with flexible spacers, a spacer chain can be considered to be a nearly unperturbed flexible polymer chain in a good solvent, and the swelling of the dendrimer is realized by deformation on larger scales. This is explicitly shown in Figure 5b, where we plot the radius of gyration of the spacers as a function of spacer length at various temperatures and generations. Therefore, small swelling ratio is dominated by rearrangement of spacers of dendrimers.

We note that spacer length invariance is not sufficient for spacer-length scaling because electrostatic effects including the effect of counterions can depend on G and S, which is in fact the case. (See for instance Figure 3.) Therefore, eq 9 has to be considered to be an empirical conclusion. Perturbation calculations of the electrostatic effects might help to understand this behavior in more detail.

C. Spatial Distribution of Monomers and Terminal Groups. In the previous section, we have shown that the spacer length scaling is nearly obeyed. (See eq 9.) Therefore, we analyze the spatial distribution of monomers in terms of the self-density of spacers. Figures 6 and 7 show the radial monomer density profiles, ρ_m, as a function of the distance from the dendrimers' c.m. at the considered reduced temperatures, τ.

In general, our simulations confirm the so-called dense core picture of terminally charged dendrimers. Actually, it is seen that for each τ, there is a high concentration of monomers close to the c.m. that corresponds to the dense core of the molecules. At larger distances, the monomer density drops sharply to a local minimum, followed by a broad maximum/plateau within the actual dendritic domain. Finally, on the periphery, ρ_m decreases to zero.

Note that according to our above arguments concerning the scaling properties of R_g the values of ρ_m and r are rescaled, as for neutral dendrimers we have previously considered,[66] which also leads to a reasonable collapse of the profiles on master curves. Therefore, for fixed G, the rescaled monomer density, $\rho_m/S^{1-3\nu}$, as a function of the rescaled radial distance, r/S^{ν}, from the dendrimers' center displays excluded volume, spacer-length scaling to a large extent, and the charge might be considered to be a weak force that leads to swelling of the uncharged dendrimer.

In Figures 8 and 9, we show that the radial density of terminal groups, ρ_e, grows from small but finite values close to the core to maximal ones in the dendritic domain and subsequently decreases to zero. The plots clearly demonstrate that the terminal groups fold back into the dendritic

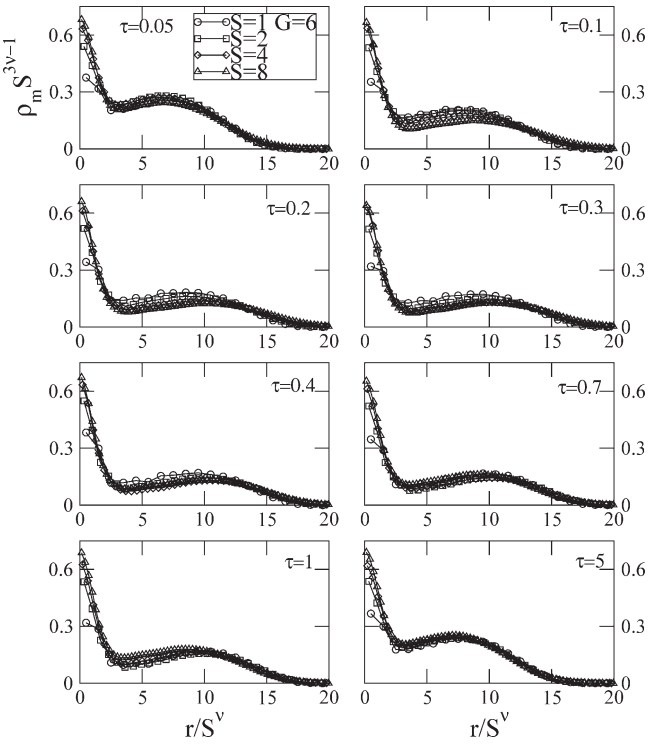

Figure 7. Rescaled radial monomer density ρ_m versus the rescaled distance from the dendrimers' c.m. at various τ for $G = 6$.

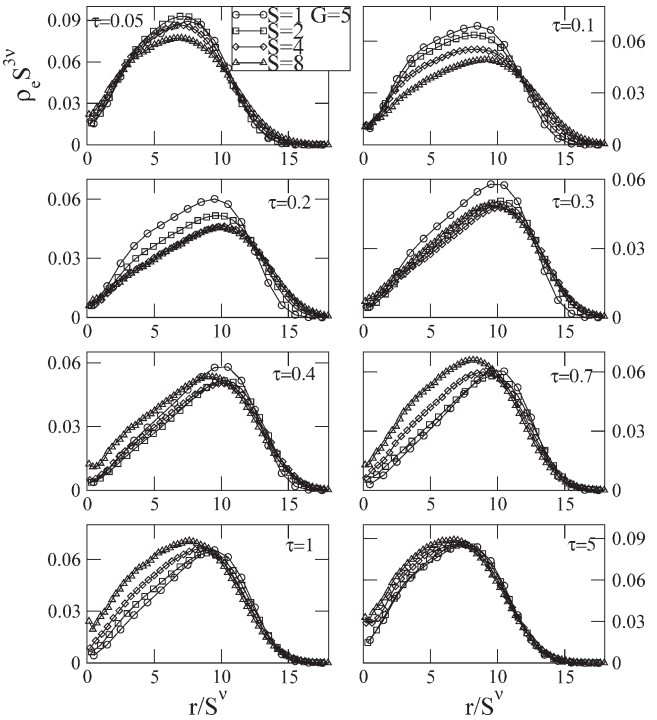

Figure 8. Rescaled radial density of terminal groups, ρ_e, versus the rescaled distance from the dendrimers' c.m. at various τ for $G = 5$.

interior. They penetrate not only the periphery but also, first of all, the molecules' domain. Note that for ρ_e, we have again applied the analogous rescaling procedure, as for ρ_m, which, however, does not result in such a good collapse of the data.[66] In the case of terminally charged dendrimers, some deviations from scaling in the region between $0.1 < \tau < 0.7$ are present.

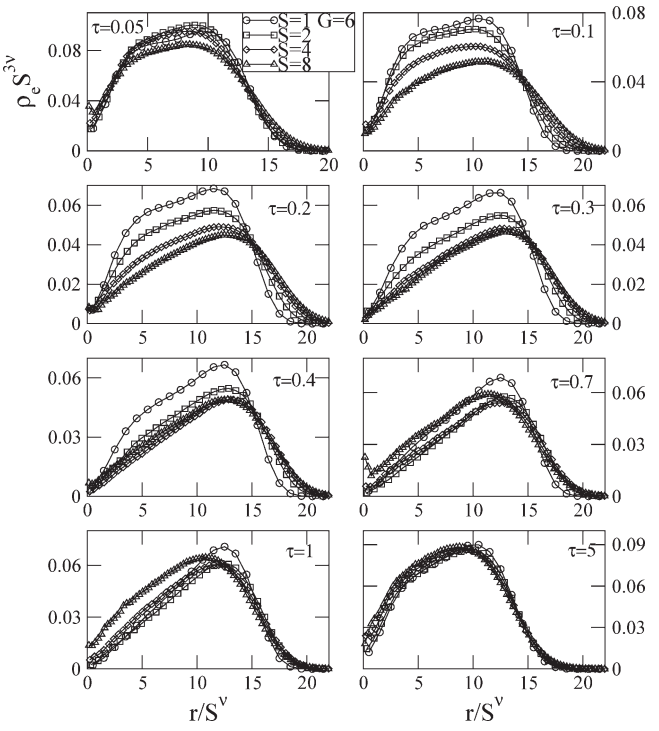

Figure 9. Rescaled radial density of terminal groups, ρ_e, versus the rescaled distance from the dendrimers' c.m. at various τ for $G = 6$.

By comparing the shape of the distribution of the terminal groups as a function of temperature, one can observe a tendency for terminal groups to stretch toward the surface of the monomer cloud at intermediate temperatures. In contrast, the distribution of all monomers changes only weakly with temperature. This indicates an "unfolding" of the terminal spacers with increasing effect of electrostatic interactions as the minimum response of the molecule. These observations confirm our conclusion that charging of terminal groups influences the conformational properties of dendrimers rather weakly.

D. Spatial Distribution of Counterions. It is generally accepted that the above presented changes in the dendrimer's size are due to counterion-imposed screening of electrostatic repulsion between the terminal groups. Specifically, as τ decreases, ions condense, causing more screening. The nonmonotonous behavior of R_g is therefore a result of the subtle interplay between the repulsion that promotes extended conformations of dendritic branches and condensation that weakens this tendency. In Figure 10, we display the counterion radial density, ρ_c, plotted versus the rescaled radial distance, r/R_g, from the dendrimer's c.m. In fact, ions penetrate all of the dendrimer volume. In accordance with strong condensation at the lowest temperatures, ρ_c is very high within the dendritic interior, where it reaches the maximum at $r \approx R_g$. We thus find that counterions are well localized in the space occupied by the dendrimer. Obviously, this tendency weakens as τ increases, and, in the extreme of high τ, ions are distributed all over the space. (See also snapshots shown in Figure 12.) Note that as presented in Figure 11, because of greater dendrimer volume for longer spacers, ρ_c is substantially reduced at given τ.

A quantitative measure of the strength of counterion localization in the dendrimer volume is also the normalized fraction, f_t, of counterions located at the distance less than R_g from the dendrimer's c.m. (See Figure 13.) As shown in Figure 13a, f_t drops from around 0.4 down to nearly 0 with

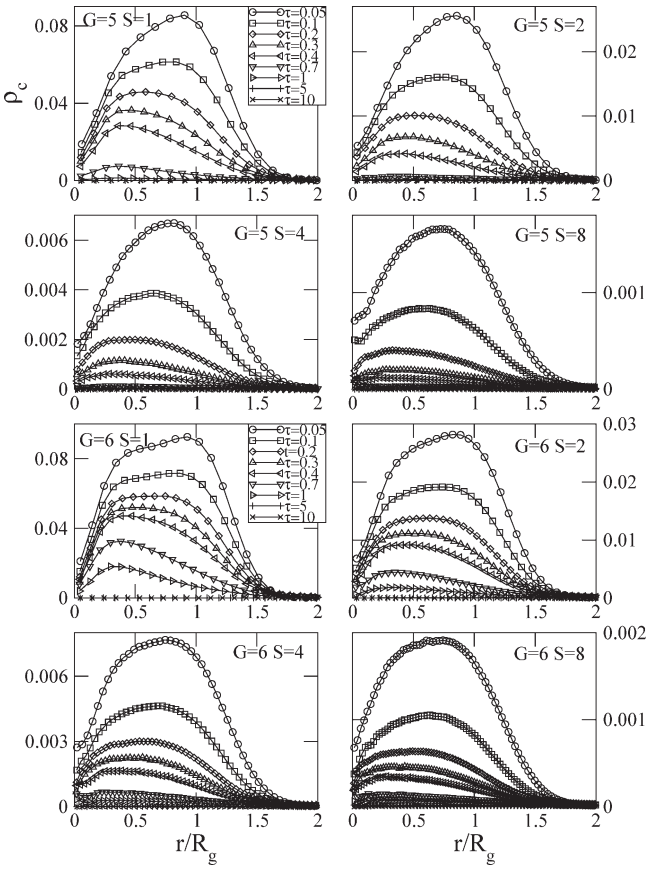

Figure 10. Radial counterion density, ρ_c, versus the rescaled distance from the dendrimers' c.m. at various τ.

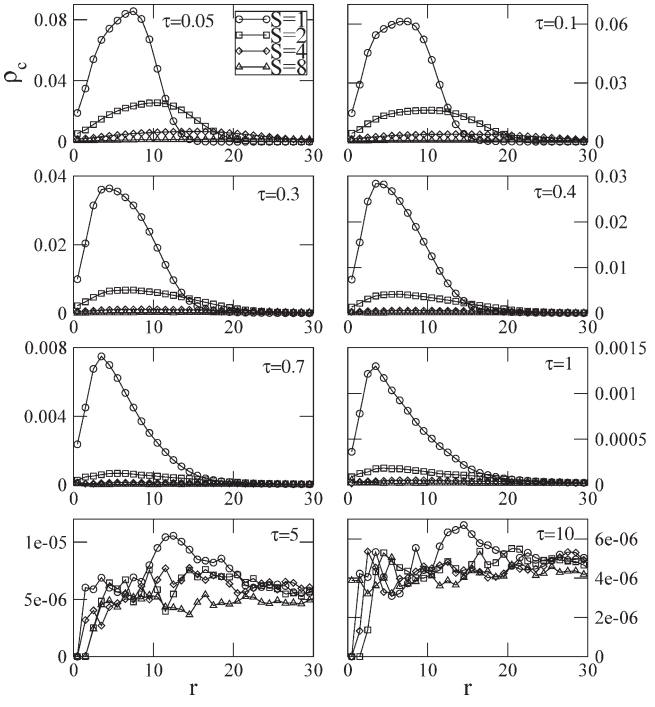

Figure 11. Radial counterion density, ρ_c, versus the distance from the dendrimers' c.m. at various S for $G = 5$.

increasing τ. More interestingly, at fixed τ and S, the fraction of trapped ions increases for the higher generation, $G = 6$, whereas for fixed τ and G, it decreases with longer spacers. (See Figure 13b.)

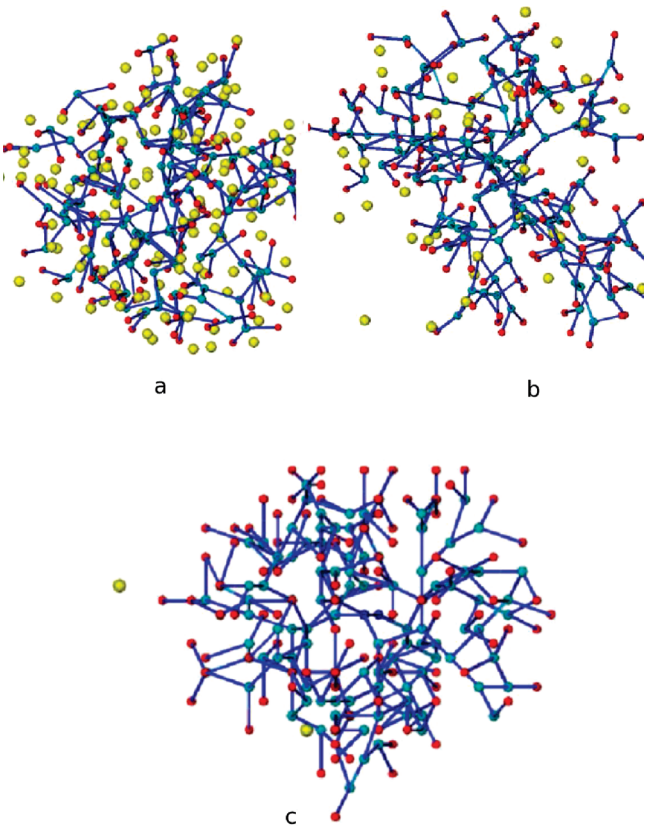

Figure 12. Snapshots of dendrimer/counterions configurations for $G = 6$ and $\tau =$ (a) 0.05, (b) 0.7, and (c) 10. The terminal groups (counterions) are shown with red (yellow) spheres.

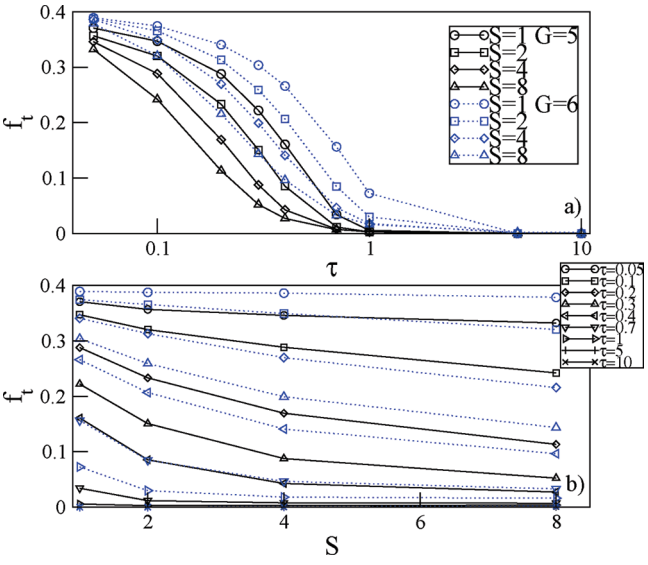

Figure 13. (a) Mean fraction of counterions, f_t, located at the distance less than R_g from the dendrimer's c.m. versus τ, (b) Mean fraction of counterions, f_t, located at the distance less than R_g from the dendrimer's c.m. versus S at fixed τ. The solid (dotted) lines correspond to $G = 5$ ($G = 6$).

Apart from the spatial distribution of counterions, it is instructive to demonstrate the mean overall charge density, $\rho_{ch} = \rho_e - \rho_c$, which is presented in Figure 14. At the lowest τ, ρ_{ch} is nearly zero because of the almost perfect condensation of counterions on the molecule. In fact, in this case, counterions are localized on the terminal groups following their distribution. Subsequently, as τ is increased, ρ_{ch} gradually becomes dominated by the contribution from the terminal groups themselves.

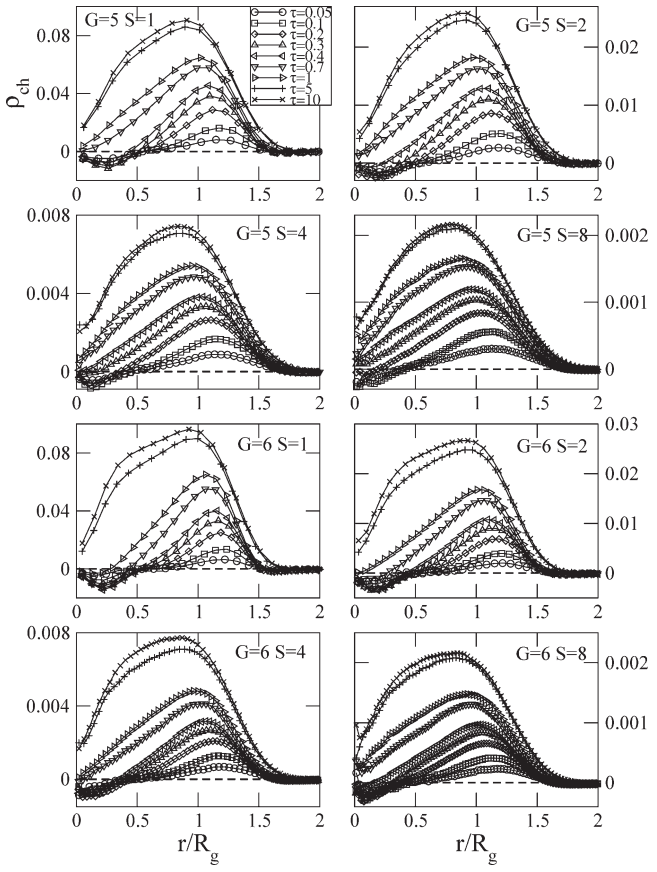

Figure 14. Overall charge density, ρ_{ch}, versus the rescaled distance from the dendrimers' c.m. r/R_g at various τ. The horizontal dashed lines correspond to $\rho_{ch} = 0$.

E. Instantaneous Shape. The instantaneous shape of a polymer molecule usually breaks spherical symmetry. A linear chain, for instance, displays a prolate ellipsoidal shape.[74,75] Note that it is important to distinguish between the shape observed with and without orientational averaging because only the latter can become aspherical in an otherwise isotropic environment. This, for instance, can play a role in such phenomenon as viscous flow or diffusion of dendrimers, which in turn may be important for applications. The question of dendrimers' shape has been directly dealt with by TEM measurements of individual dendrimer molecules of poly(amidoamine) (PAMAM), and from the stained images, it has been concluded that to a first approximation, dendrimers of generations between $G = 7$ and 10 are spherical in shape, although a more detailed inspection suggests that they are rather polyhedronlike objects.[76] Moreover, some simulation studies complement the experiment and indicate asymmetric shapes of dendrimers of low generations, G, and nearly spherical shapes of molecules of higher G.[77−80]

The instantaneous shape of polymers can be quantitatively analyzed by means of the radius of gyration tensor[74,77,81]

$$R_{\mu\nu} = (1/N)\left[\sum_i^N (r_{\mu i} - r_{\mathrm{cm},\mu})(r_{\nu i} - r_{\mathrm{cm},\nu})\right], \mu, \nu = x, y, z \quad (11)$$

where $r_{\mu i}$ and $r_{\mathrm{cm},\mu}$ are the coordinates of the ith monomer and of the center of mass of the molecule in the laboratory frame of reference, respectively. From the definition (eq 11), it follows that $R_{\mu\nu}$ is real and symmetric; therefore, it can be diagonalized by a linear transformation to the principial axis system, in

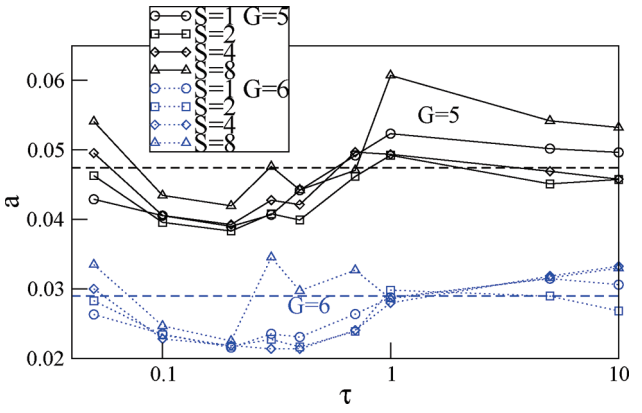

Figure 15. Shape anisotropy, a, versus τ. The solid (dotted) lines correspond to $G = 5$ ($G = 6$). The dashed horizontal lines show a for neutral dendrimers of corresponding generations with $S = 1$.

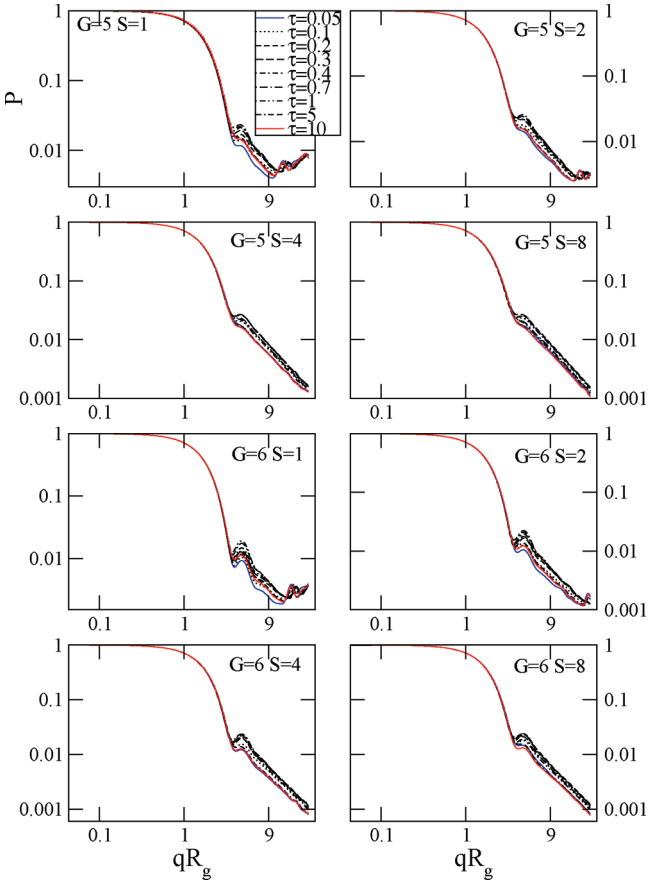

Figure 16. Form factor for fixed G and S at various τ.

which the eigenvalues I_x, I_y, and I_z of $R_{\mu\nu}$ are real and positive. These eigenvalues correspond to semiaxes of 3D ellipsoides that within this kind of approach represent polymers. More specifically, two invariants (I_1 and I_2) of $R_{\mu\nu}$ out of the three

$$I_1 = Tr(R_{\mu\nu}) = I_x + I_y + I_z = R_g^2,$$
$$I_2 = I_xI_y + I_xI_z + I_yI_z, \quad I_3 = I_xI_yI_z \quad (12)$$

where R_g stands for the radius of gyration, are used to define the so-called relative shape anisotropy[74,77,81]

$$a = 1 - 3I_2/I_1^2 \quad (13)$$

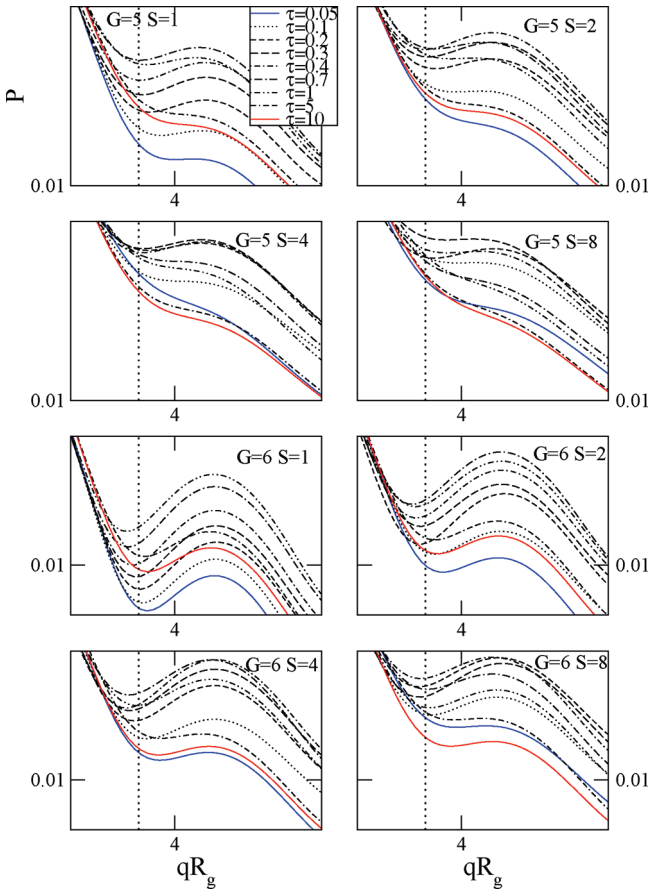

Figure 17. Form factor for fixed G and S at various τ for $3 \leq qR_g \leq 6$. The vertical dotted line refers to $qR_g = 3.62$.

which takes values between 0 and 1. In particular, $a = 0$, 1/4, and 1 for spherical, oblate, and extremely elongated ellipsoides, respectively. Note that the calculation of the ensemble averages of the above quantities requires that $R_{\mu\nu}$ is diagonalized in every stored equilibrium conformation.

In Figure 15, we show the average relative shape anisotropy, a, as a function of the reduced temperature, τ. Although a is smaller for the molecule of higher generation $G = 6$, generally speaking in the whole range of τ, both of them are rather isotropic in shape because a is of the order of 10^{-2}. For given generation, the dependence of a on spacer length is rather minor, and the actual value of a is determined by the generation itself. Therefore, we conclude that it is rather the generation number and not the spacer length that controls the instantaneous shape of terminally charged dendrimers. The molecules we inspect in our studies are spherical.

F. Form Factor. Scattering techniques such as SANS[8,34,82,83] and SAXS[84−87] are used to study dendrimers' conformations experimentally. In the case of dilute solutions, they provide scattering dominated by the contribution of a single molecule. More specifically, it is the form factor $P(q)$ of single dendrimers that can be both measured in experiments and calculated in simulations. This quantity is defined as

$$P(q) = \frac{1}{N^2}\left\langle \sum_i^N \sum_j^N \frac{\sin(qr_{ij})}{qr_{ij}} \right\rangle \qquad (14)$$

where q is the magnitude of the scattering vector and r_{ij} is the distance between beads i and j, whereas the angular brackets denote ensemble averaging.

Our simulation results concerning $P(q)$ for various S and τ are shown in Figure 16. In particular, for dendrimers with spacers $S = 4$ and 8, they are in qualitative agreement with those recently obtained from SANS experiments with charged G4 PAMAM molecules in aqueous solutions.[8]

The striking feature of dendrimer form factors is the appearance of oscillations in the high qR_g range, which are typical both for neutral and charged molecules of higher generations and show up because of dendrimers' sharper boundaries.[8,34,56,84,87,88] Of particular interest is the position of the first minimum of the scattering curves that yields the overall size of dendrimers. Our data presented in Figure 17 show that the positions of the first minimums hardly depend on τ and appear at $qR_g \approx 3.62$, which is the characteristic value for the location of the first minimum of the form factor of a uniform sphere with the radius of gyration, R_g. The plots we present do not reveal oscillations of higher order, indicating a rather open structure in contrast with a dense sphere or shell.

IV. Conclusions

We have used the bond fluctuation model to investigate terminally charged dendrimers with flexible spacers with long-range electrostatic interactions and explicit treatment of counterions over a wide range of temperatures. Our model has been chosen to mimic dendritic polyelectrolytes such as PAMAM at neutral pH values where only the terminal groups are dissociated.

We have shown that the presence of charged end groups does not lead to strong deviations in comparison with the properties of neutral dendrimers within the range of temperatures we have studied. The size of terminally charged dendrimers displays nonmonotonous behavior as a function of temperature with a maximum volume swelling factor of about two. At very low temperature, counterion condensation at the terminal groups leads to effective neutral behavior of the dendrimer, whereas at large temperatures, electrostatic interactions contribute only weakly to the free energy of the molecules. We found that the swelling effect is dominated by temperature, and effects of generation and spacer-length play only a minor role. As a consequence, spacer-length scaling as predicted and observed for neutral dendrimers is approximately obeyed for terminally charged dendrimers as well. In accordance with this conclusion, the averaged extension of spacer chains is nearly invariant with respect to variation of generation and temperature. Swelling of terminally charged dendrimers is mainly due to unfolding of the branched structure, in particular, of the terminal spacer rather than stretching of spacers. Larger deviations from spacer-length scaling, however, can be found for the distribution of terminal groups, which tend to be more localized on the surface of the molecule at intermediate temperature due to electrostatic interactions. The present study indicates that the sensitivity of the dendrimers' size with respect to temperature or strength of dielectric medium can be described in a scalable way independent of the spacer length. This opens the possibility of synthesizing dendrimers of various size with a predictable behavior.

As for neutral dendrimers, terminally charged dendrimers display a dense-core distribution of monomers and backfolding of terminal groups into the interior of the molecules' volume. The instantaneous shape of the dendrimers displays only weak anisotropy. The scattering factors indicate an onset of oscillating behavior at high values of the scattering vector for generation six, which, however, should not be mistaken as a form factor of a dense sphere or shell.

In conclusion, our results indicate the dominance of excluded volume effects in athermal solvent and that charge effects might be described as a correction to neutral behavior. Swelling effects can even be weakened in the presence of salt. This can be a

fortunate situation when considering interactions of terminally charged dendrimers with other charged objects because simple mean-field and scaling arguments developed for neutral dendrimers can be applied to understand the dendrimers' behavior in this case. Stronger charging of dendrimers such as charging branching points may be necessary to observe a behavior dominated by electrostatic effects.

Acknowledgment. Support from the Deutsche Forschungsgemeinschaft (DFG) contract number SO-277/2-1 is gratefully acknowledged. Part of the calculations were carried out at the Center for High Performance Computing (ZIH) of the TU Dresden.

Appendix A: The Ewald Sum

The total interaction energy of a solution of N ions with valences z_i and positions $\mathbf{r}_i$ in the cubic box of size L^3 with periodical boundaries is given by[69,70]

$$E = \frac{E_c(\mathrm{r}_i)}{\delta} = \frac{1}{2}{\sum_{\mathrm{k}}}' \sum_{i=1}^{N}\sum_{j=1}^{N} \frac{z_i z_j}{|\mathrm{r}_{ij} + L\mathbf{k}|} \tag{15}$$

where $\delta = e^2/\varepsilon u$, e, ε, and u stand for the electric charge, permittivity of the solvent, and length unit, respectively. The first sum in eq 15 is over all integer vectors, $\mathbf{k}$, and the prime indicates that for $\mathbf{k} = 0$, terms with $i = j$ must be skipped. In other words, except for self-interactions, both the interactions between the charges in the central box and those between them and their replicas contribute to E. The sum eq 15 is conditionally convergent, which means that its value depends on the order the terms are added.

The Ewald formula for a neutral, periodic system of charges surrounded by a conducting medium is based on the addition of contributions from the replicas in the order of their distance from the central box. The final result is given by

$$E = \sum_{1\le i<j\le N} \frac{z_i z_j \,\mathrm{erfc}(k r_{ij})}{r_{ij}} - \frac{\kappa}{\sqrt{\pi}}\sum_{j=1}^{N} z_j^2 + \frac{1}{2\pi L}\sum_{\mathbf{k}\neq 0}\left[\frac{1}{k^2}\exp\left(-\frac{\pi^2 k^2}{L^2\kappa^2}\right)\left|\sum_{j=1}^{N} z_j \exp\left(\frac{2\pi i}{L}\,\mathbf{k}\cdot\mathbf{r}_j\right)\right|^2\right] \tag{16}$$

where

$$\mathrm{erfc}(x) = \frac{2}{\sqrt{\pi}}\int_x^\infty \exp(-t^2)\,\mathrm{d}t \tag{17}$$

is the complementary error function and κ is a parameter whose value is determined by the numerical accuracy. Therefore, the calculation of E involves summation of the pairwise short-range potential in the real space and one over Fourier space, respectively. In practice, some cutoff r_c on the real-space potential together with periodic boundaries and truncation, $|\mathbf{k}| \le k_{max}$, in the sum over Fourier vectors are imposed such that both contributions produce errors of the same order. In typical, κ and r_c are set to $5/L$ and $L/2$, respectively, which leads to $k_{max} \approx 5$.

References and Notes

(1) DeLong, R.; Stephenson, K.; Loftus, T.; Fisher, M.; Alahari, S.; Nolting, A.; Juliano, R. L. *J. Pharm. Sci.* **1997**, *86*, 762.
(2) Yoo, H.; Sazani, P.; Juliano, R. L. *Pharm. Res.* **1999**, *16*, 1799.
(3) Kukowska-Latallo, J. F.; Bielinska, A.; Johnson, J.; Spindler, R.; Tomalia, D. A.; Baker, J. R. *Proc. Natl. Acad. Sci. U.S.A.* **1996**, *93*, 4897.
(4) Khan, M. K.; Nigavekar, S. S.; Minc, L. D.; Kariapper, M. S. T.; Nair, B. M.; Lesniak, W. G.; Balogh, L. P. *Technol. Cancer Res. Treat.* **2005**, *4*, 603.
(5) Ohshima, A.; Konishi, T.; Yamanaka, J.; Ise, N. *Phys. Rev. E* **2001**, *64*, 051808.
(6) Young, J. K.; Baker, G. R.; Newkome, G. R.; Morris, K. F.; Johnson, J. C. S. *Macromolecules* **1994**, *27*, 3464.
(7) Ramzi, A.; Scherrenberg, R.; Joosten, J.; Lemstra, P.; Mortensen, K. *Macromolecules* **2002**, *35*, 827.
(8) Chen, W.; Porcar, L.; Liu, Y.; Butler, P. D.; Magid, L. J. *Macromolecules* **2007**, *40*, 5887.
(9) Gröhn, F.; Bauer, B. J.; Akpalu, Y. A.; Jackson, C. L.; Amis, E. J. *Macromolecules* **2000**, *33*, 6042.
(10) Gröhn, F.; Kim, G.; Bauer, B. J.; Amis, E. J. *Macromolecules* **2001**, *34*, 2179.
(11) Ottaviani, M. F.; Montalti, F.; Turro, N. J.; Tomalia, D. *J. Phys. Chem. B* **1997**, *101*, 158.
(12) Vassilev, K.; Ford, W. T. *J. Polym. Sci., Part A: Polym. Chem.* **1999**, *37*, 2727.
(13) Lin, W.; Galletto, P.; Borkovec, M. *Langmuir* **2004**, *20*, 7465.
(14) Cahill, B. P.; Papastavrou, G.; Koper, G. J. M.; Borkovec, M. *Langmuir* **2008**, *24*, 465.
(15) Pericet-Camara, R.; Papastavrou, G.; Borkovec, M. *Macromolecules* **2009**, *42*, 1749.
(16) Reinhold, F.; Kolb, U.; Lieberwirth, I.; Gröhn, F. *Langmuir* **2009**, *25*, 1345.
(17) Dünweg, B.; Stevens, M.; Kremer, K. In *Monte Carlo and Molecular Dynamics Simulations in Polymer Science*; Binder, K., Ed.; Oxford University Press: New York, 1995.
(18) Hayashi, Y.; Ullner, M.; Linse, P. *J. Chem. Phys.* **2002**, *116*, 6836.
(19) Lobaskin, V.; Linse, P. *J. Chem. Phys.* **1998**, *109*, 3530.
(20) Limbach, H. J.; Holm, C. *Comput. Phys. Commun.* **2002**, *147*, 321.
(21) Limbach, H. J.; Holm, C. *J. Chem. Phys.* **2001**, *114*, 9674.
(22) Manning, G. S. *J. Chem. Phys.* **1969**, *51*, 924.
(23) Manning, G. S. *J. Chem. Phys.* **1969**, *51*, 934.
(24) Manning, G. S. *J. Chem. Phys.* **1969**, *51*, 3249.
(25) Manning, G. S. *J. Chem. Phys.* **1988**, *89*, 3773.
(26) Winkler, R. G.; Gold, M.; Reineker, P. *Phys. Rev. Lett.* **1998**, *80*, 3731.
(27) Hofmann, T.; Winkler, R. G.; Reineker, P. *J. Chem. Phys.* **2001**, *114*, 10181.
(28) Liu, S.; Muthukumar, M. *J. Chem. Phys.* **2002**, *116*, 9975.
(29) Chang, R.; Yethiraj, A. *J. Chem. Phys.* **2003**, *118*, 6634.
(30) Chang, R.; Yethiraj, A. *J. Chem. Phys.* **2003**, *118*, 11315.
(31) Stevens, M. J.; Kremer, K. *J. Chem. Phys.* **1995**, *103*, 1669.
(32) Kreisel, J. W.; König, S.; Freitas, M. A.; Marshall, A. G.; Leary, J. A.; Tilley, T. D. *J. Am. Chem. Soc.* **1998**, *120*, 12207.
(33) Welch, C. F.; Hoagland, D. A. *Langmuir* **2003**, *19*, 1082.
(34) Nisato, G.; Ivkov, R.; Amis, E. J. *Macromolecules* **2000**, *33*, 4172.
(35) Rahman, K. M. A.; Durning, C. J.; Turro, N. J.; Tomalia, D. A. *Langmuir* **2000**, *16*, 10154.
(36) Li, X.; Imae, T.; Leisner, D.; López-Quintela, M. A. *J. Phys. Chem. B* **2002**, *106*, 12170.
(37) Zhang, H.; Dubin, P. L.; Ray, J.; Manning, G. S.; Moorefield, C. N.; Newkome, G. R. *J. Phys. Chem. B* **1999**, *103*, 2347.
(38) Leisner, D.; Imae, T. *J. Phys. Chem. B* **2004**, *108*, 1798.
(39) Bosko, J. T.; Todd, B. D.; Sadus, R. J. *J. Chem. Phys.* **2004**, *121*, 1091.
(40) Galperin, D. E.; Ivanov, V. A.; Mazo, M. A.; Khokhlov, A. R. *Polym. Sci. Ser. A* **2005**, *47*, 61.
(41) Gurtovenko, A. A.; Lyulin, S. V.; Karttunen, M.; Vattulainen, L. *J. Chem. Phys.* **2006**, *124*, 094904.
(42) Lee, I.; Athey, B. D.; Wetzel, A. W.; Meixner, W.; Baker, J. J. R. *Macromolecules* **2002**, *35*, 4510.
(43) Maiti, P. K.; Çağin, T.; Lin, S.; Goddard, I. W. A. *Macromolecules* **2005**, *38*, 979.
(44) Majtyka, M.; Kłos, J. *Phys. Chem. Chem. Phys.* **2007**, *9*, 2284.
(45) Majtyka, M.; Kłos, J. *J. Phys.: Condens. Matter* **2006**, *18*, 3581.
(46) Majtyka, M.; Kłos, J. *Acta Phys. Pol., A* **2006**, *110*, 833.
(47) Terao, T.; Nakayama, T. *Macromolecules* **2004**, *37*, 4686.
(48) Terao, T. *Mol. Phys.* **2006**, *105*, 2507.
(49) Paulo, P. M. R.; Lopes, J. N. C.; Costa, S. M. B. *J. Phys. Chem. B* **2007**, *111*, 10651.
(50) Lyulin, S. V.; Vattulainen, I.; Gurtovenko, A. A. *Macromolecules* **2008**, *41*, 4961.
(51) Karatasos, K. *Macromolecules* **2008**, *41*, 1025.
(52) Karatasos, K.; Krystallis, M. *Macromol. Symp.* **2009**, *278*, 32.
(53) Karatasos, K.; Krystallis, M. *J. Chem. Phys.* **2009**, *130*, 114903.

(54) Blaak, R.; Lehmann, S.; Likos, C. N. *Macromolecules* **2008**, *41*, 4452.
(55) Tian, W.; Ma, Y. *J. Phys. Chem. B* **2009**, *113*, 13161.
(56) Lin, Y.; Liao, Q.; Jin, X. *J. Phys. Chem. B* **2007**, *111*, 5819.
(57) Welch, P.; Muthukumar, M. *Macromolecules* **1998**, *31*, 5892.
(58) Lyulin, S. V.; Evers, L. J.; van der Schoot, P.; Darinskii, A. A.; Lyulin, A. V.; Michels, M. A. *Macromolecules* **2004**, *37*, 3049.
(59) Lyulin, S. V.; Darinskii, A. A.; Lyulin, A. V.; Michels, M. A. *Macromolecules* **2004**, *37*, 4676.
(60) Suman, B.; Kumar, S. *J. Phys. Chem. B* **2007**, *111*, 8728.
(61) Welch, P.; Muthukumar, M. *Macromolecules* **2000**, *33*, 6159.
(62) Lyulin, S. V.; Darinskii, A. A.; Lyulin, A. V. *Macromolecules* **2005**, *38*, 3990.
(63) Lyulin, S. V.; Lyulin, A. V.; Darinskii, A. A.; Emri, I. *Polym. Sci., Ser. A* **2005**, *47*, 1217.
(64) Lyulin, S. V.; Darinskii, A. A.; Lyulin, A. V. *Phys. Rev. E* **2008**, *78*, 041801.
(65) Wolterink, J. K.; van Male, J.; Daoud, M.; Borisov, O. V. *Macromolecules* **2003**, *36*, 6624.
(66) Kłos, J. S.; Sommer, J.-U. *Macromolecules* **2009**, *42*, 4878.
(67) Carmesin, I.; Kremer, K. *Macromolecules* **1988**, *21*, 2819.
(68) Trautenberg, H. L.; Hölzl, T.; Göritz, D. *Comput. Theor. Polym. Sci.* **1996**, *6*, 135.
(69) Allen, M. P.; Tildesley, D. J. *Computer Simulation of Liquids*; Clarendon Press: Oxford, U.K., 1984.
(70) Rapaport, D. C. *The Art of Molecular Dynamics Simulation*, 2nd ed.; Cambridge University Press: Cambridge, U.K., 2004.
(71) Pavlov, G. M.; Korneeva, E. V.; Meijer, E. W. *Colloid Polym. Sci.* **2002**, *280*, 416.
(72) Meropolis, A. W.; Rosenbluth, N. N.; Rosenbluth, A. H.; Teller; Teller, E. *J. Chem. Phys.* **1953**, *21*, 1087.
(73) Grass, K.; Holm, C. *Soft Matter* **2009**, *5*, 2079.
(74) Theodoru, D. N.; Suter, U. *Macromolecules* **1985**, *18*, 1206.
(75) Doi, M.; Edwards, S. F. *The Theory of Polymer Dynamics*, 2nd ed.; Oxford University Press: Oxford, U.K., 1998.
(76) Jackson, C. L.; Chanzy, H. D.; Booy, F. P.; Drake, B. J.; Tomalia, D. A.; Bauer, B. J.; Amis, E. J. *Macromolecules* **1998**, *31*, 6259.
(77) Maiti, P. K.; Çağin, T.; Wang, G.; Goddard, W., III. *Macromolecules* **2004**, *37*, 6236.
(78) Naylor, A. M.; Goddard, W. A.; Keiffer, G. E.; Tomalia, D. A. *J. Am. Chem. Soc.* **1989**, *111*, 2339.
(79) Mansfield, M. L.; Klushin, L. I. *Macromolecules* **1993**, *26*, 4262.
(80) Karatasos, K.; Adolf, D. B.; Davies, G. R. *J. Chem. Phys.* **2001**, *115*, 5310.
(81) Rudnick, J.; Gaspari, G. *J. Phys. A: Math. Gen.* **1986**, *19*, L191.
(82) Pötschke, D.; Ballauff, M.; Lindner, P.; Fischer, M.; Vögtle, F. *Macromolecules* **1999**, *32*, 4079.
(83) Rosenfeldt, S.; Dingenouts, N.; Ballauff, M.; Werner, N.; Vögtle, F.; Lindner, P. *Macromolecules* **2002**, *35*, 8098.
(84) Prosa, T. J.; Bauer, B. J.; Amis, E. J. *Macromolecules* **2001**, *34*, 4897.
(85) Prosa, T. J.; Bauer, B. J.; Amis, E. J.; Tomalia, D. A.; Scherrenberg, R. *J. Polym. Sci., Part B: Polym. Phys.* **1997**, *35*, 2913.
(86) Rathgeber, S.; Pakula, T.; Urban, V. *J. Chem. Phys.* **2004**, *121*, 3840.
(87) Rathgeber, S.; Monkenbusch, M.; Kreitschmann, M.; Urban, V.; Brulet, A. *J. Chem. Phys.* **2002**, *117*, 4047.
(88) Götze, O.; Likos, C. *Macromolecules* **2003**, *36*, 8189.